

Isospectralization, or how to hear shape, style, and correspondence

Luca Cosmo
University of Venice
luca.cosmo@unive.it

Mikhail Panine
École Polytechnique
mpanine@lix.polytechnique.fr

Arianna Rampini
Sapienza University of Rome
rampini@di.uniroma1.it

Maks Ovsjanikov
École Polytechnique
maks@lix.polytechnique.fr

Michael M. Bronstein
Imperial College London / USI
m.bronstein@imperial.ac.uk

Emanuele Rodolà
Sapienza University of Rome
emanuele.rodola@uniroma1.it

Abstract

The question whether one can recover the shape of a geometric object from its Laplacian spectrum (‘hear the shape of the drum’) is a classical problem in spectral geometry with a broad range of implications and applications. While theoretically the answer to this question is negative (there exist examples of iso-spectral but non-isometric manifolds), little is known about the practical possibility of using the spectrum for shape reconstruction and optimization. In this paper, we introduce a numerical procedure called isospectralization, consisting of deforming one shape to make its Laplacian spectrum match that of another. We implement the isospectralization procedure using modern differentiable programming techniques and exemplify its applications in some of the classical and notoriously hard problems in geometry processing, computer vision, and graphics such as shape reconstruction, pose and style transfer, and dense deformable correspondence.

1. Introduction

Can one hear the shape of the drum? This classical question in spectral geometry, made famous by Mark Kac’s eponymous paper [18], inquires the possibility of recovering the structure of a geometric object from its Laplacian spectrum. Empirically, the relation between shape and its acoustic properties has long been known and can be traced back at least to medieval bellfounders. However, while it is known that the spectrum carries many geometric and topological properties of the shape such as the area, total curvature, number of connected components, etc., it is now known that one cannot ‘hear’ the metric. Examples of high-dimensional manifolds that are isospectral but not isometric have been constructed in 1964 [23] (predating Kac’s paper), but it took until 1992 to produce a counter-example of 2D polygons giving a negative answer to Kac’s ques-

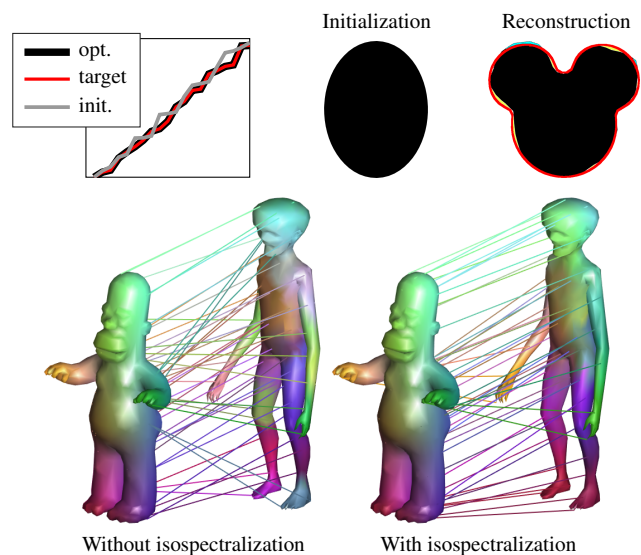


Figure 1. *Top row*: Mickey-from-spectrum: we recover the shape of Mickey Mouse from its first 20 Laplacian eigenvalues (shown in red in the leftmost plot) by deforming an initial ellipsoid shape; the ground-truth target embedding is shown as a red outline on top of our reconstruction. *Bottom row*: Aligning the Laplacian eigenvalues (‘isospectralization’) can be used as a preconditioning step for non-isometric deformable shape matching. We show the correspondence obtained with a baseline matching algorithm before (left) and after (right) isospectralization. Corresponding points are depicted with same color.

tion [13, 12].

Nevertheless, the question of relation between shape and spectrum is far from being closed, from both theoretical and practical perspectives. Specifically, it is not yet certain whether the counterexamples are the rule or the exception. So far, everything points towards the latter. In fact, there are known classes of manifolds in which the spectral reconstruction is generically possible. See [35, 36, 37, 15] for such results. Thus, it is plausible that the theoretical existence of rather ‘exotic’ counter-examples of non-isometric

isospectral manifolds does not preclude the possibility of reconstructing the shape from spectrum *in practice*.

This is exactly the direction explored in our paper. We introduce a numerical procedure we call *isospectralization*, which consists in deforming a mesh in order to align its (finite) Laplacian spectrum with a given one. We implement this procedure using modern differentiable programming tools used in deep learning applications and show its usefulness in some of the fundamental problems in geometry processing, computer vision, and graphics.

For example, we argue that isospectralization (with some additional priors such as smoothness and enclosed volume) can in some cases be used to recover the structure of an object from spectrum, thus practically hearing the shape of the drum (see Figure 1, top row).

Outside of the rare counterexamples, the reconstruction is ambiguous up to intrinsic isometry. This ambiguity manifests itself as a choice of an embedding of the mesh into \mathbb{R}^3 . This enables us to use the isospectralization procedure to transfer style and pose across objects similarly to [8]: we initialize with a source shape and apply isospectralization to obtain the eigenvalues of the target shape; the result is a shape in the pose of the source shape but with geometric details of the target.

Even more remarkably, we show that pre-warping non-isometric shapes by means of isospectralization can significantly help in solving the problem of finding intrinsic correspondences between them (Figure 1, bottom row), suggesting that our procedure could be a universal pre-processing technique for general correspondence pipelines.

Contribution. We consider the shape-from-eigenvalues problem and investigate its relevance in a selection of problems from computer vision and graphics. Our key contributions can be summarized as follows:

- Despite being highly non-linear and hard to compute, we show for the first time that the inverse mapping between a geometric domain and its Laplacian spectrum is addressable with modern numerical tools;
- We propose the adoption of simple regularizers to drive the spectrum alignment toward *globally optimal* solutions;
- We showcase our method in the 2D and 3D settings, and show applications of style transfer and dense mapping of non-isometric deformable shapes.

2. Related work

The possibility of reconstructing shape from spectrum is of interest in theoretical physics [19], and has been explored by theoreticians since the '60s starting from Leon Green's question if a Riemannian manifold is fully determined by

its (complete) spectrum [3]. The isospectrality vs isometry question received a negative answer in the seminal work of Milnor [23], and additional counterexamples were provided by Kac [18] and Gordon *et al.* [13] to name some classical examples. A complete survey of the theoretical literature on the topic is out of the scope of this paper; below, we only consider the far less well-explored *practical* question of how to realize metric embeddings from the sole knowledge of the (finite) Laplacian eigenvalues.

A related but more general class of problems takes the somewhat misleading name of *inverse eigenvalue problems* [10], dealing with the reconstruction of a generic physical system from prescribed spectral data. Different formulations of the problem exist depending on the matrix representation of the system; in the majority of cases, however, at least partial knowledge on the *eigenvectors* is also assumed.

In the fields of computer vision and geometry processing, Reuter *et al.* [28, 29] investigated the informativeness of the Laplacian eigenvalues for the task of 3D shape retrieval. The authors proposed to employ the Laplacian spectrum as a global shape signature (dubbed the 'shape DNA'), demonstrating good accuracy in distinguishing different shape classes. However, measuring the extent to which eigenvalues carry geometric and topological information about the shape was left as an open question.

More recently, there have been attempts at reconstructing 3D shapes from a full Laplacian matrix or other intrinsic operators [8, 11]. Such methods differ from our approach in that they leverage the *complete* information encoded in the input operator matrix, while we only assume to be given the operator's eigenvalues as input. Further, these approaches follow a two-step optimization process, in which the Riemannian metric (edge lengths in the discrete case) is first reconstructed from the input matrix, and an embedding is obtained in a second step. As we will show, we operate "end-to-end" by solving directly for the final embedding. It is worthwhile to mention that the problem of reconstructing a shape from its metric is considered a challenging problem in itself [7, 9]. In computer graphics, several shape modeling pipelines involve solving for an embedding under a *known* mesh connectivity and additional extrinsic information in the form of user-provided positional landmarks [31].

More closely related to our problem is the shape registration method of [14, 16]. The authors propose to solve for a conformal rescaling of the metric of two given surfaces, so that the resulting eigenvalues align well. While this approach shares with ours the overall objective of aligning spectra, the underlying assumption is for the Laplacian matrices and geometric embeddings to be given. A similar approach was recently proposed in the conformal pre-warping technique of [30] for shape correspondence using functional maps.

A related, but different, inverse spectral problem has

been tackled in [4]. There, the task is to optimize the shape of metallophone keys to produce a desired sound when struck in a specific place. Prescribing the sound consists in prescribing a sparse selection of frequencies (eigenvalues) and the amplitudes to which the frequencies are excited when the key is struck. It is also desirable that the other frequencies be suppressed. This is different from the reconstruction pursued in our work. In particular, the desired eigenvalues are not prescribed a particular position in the spectrum, they are merely required to be present somewhere in the spectrum. This is different from our approach in that we prescribe a precise sequence of eigenvalues. Further, amplitude suppression is implemented by designing the nodal sets of specific *eigenfunctions*, thus bringing this type of approach closer to a partially described inverse eigenvalue problem [10, Chapter 5].

Perhaps most closely related to our approach are methods that have explored the possibility of reconstructing shapes from their spectrum in the case of coarsely triangulated surfaces [1] and planar domains [27]. These works also indicate that non-isometric isospectral shapes are exceedingly rare. Compared to the present paper, [1] and [27] study shapes with a low number of degrees of freedom. There, the shapes are prescribed by fewer than 30 parameters, while we allow every vertex in the mesh to move.

3. Background

Manifolds. We model a shape as a compact connected 2-dimensional Riemannian manifold \mathcal{X} (possibly with boundary $\partial\mathcal{X}$) embedded either in \mathbb{R}^2 (flat shape) or \mathbb{R}^3 (surface). The intrinsic gradient ∇ and the positive semi-definite Laplace-Beltrami operator Δ on \mathcal{X} generalize the corresponding notions of gradient and Laplacian from Euclidean spaces to manifolds. In particular, Δ admits a spectral decomposition

$$\Delta\varphi_i(x) = \lambda_i\varphi_i(x) \quad x \in \text{int}(\mathcal{X}) \quad (1)$$

$$\langle \nabla\varphi_i(x), \hat{n}(x) \rangle = 0 \quad x \in \partial\mathcal{X}, \quad (2)$$

with homogeneous Neumann boundary conditions (2); here \hat{n} denotes the normal vector to the boundary.

Spectrum. The *spectrum* of \mathcal{X} is the sequence of eigenvalues of its Laplacian. These form a discrete set, which is a canonically ordered non-decreasing sequence:

$$0 = \lambda_1 < \lambda_2 \leq \dots, \quad (3)$$

where λ_1 has multiplicity 1 due to the connectedness of \mathcal{X} ; for $i > 1$, the multiplicity of λ_i is related to the intrinsic symmetries of \mathcal{X} . The growth rate of the ordered sequence (λ_i) is further related to the total surface area of \mathcal{X} via Weyl's asymptotic law [34]:

$$\lambda_i \sim \frac{4\pi}{\int_{\mathcal{X}} dx} i, \quad i \rightarrow \infty. \quad (4)$$

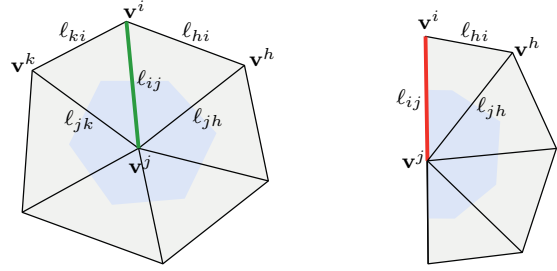


Figure 2. Notation used in this paper. Edge e_{ij} has length ℓ_{ij} ; triangle F_{ijk} has area A_{ijk} . The shaded polygon denotes the local area element a_j at vertex v_j .

This result makes it clear that shape can be directly deduced from the spectrum (*i.e.*, one can “hear the size” of the drum). This fact can be used in a reconstruction algorithm, for example, by providing an initial embedding having approximately the sought area.

Discretization. In the discrete setting, our shapes \mathcal{X} are approximated by manifold triangle meshes $X = (V, E, F)$ sampled at vertices $V = \{v_1, \dots, v_n\}$, and where each edge $e_{ij} \in E_i \cup E_b$ belongs to at most two triangle faces F_{ijk} and F_{jih} . We denote by E_i and E_b the interior and boundary edges, respectively. The discrete Riemannian metric is defined by assigning a length $\ell_{ij} > 0$ to each edge $e_{ij} \in E$; see Figure 2 for the notation.

A d -dimensional *embedding* for X is realized by assigning coordinates in \mathbb{R}^d to the vertices V ; these are encoded in a $n \times d$ matrix \mathbf{V} containing d -dimensional vertex coordinates \mathbf{v}^i for $i = 1, \dots, n$ as its rows. Edge lengths can thus be written in terms of \mathbf{V} as:

$$\ell_{ij}(\mathbf{V}) = \|\mathbf{v}^i - \mathbf{v}^j\|_2 \quad (5)$$

for all $e_{ij} \in E$.

The discrete Laplace-Beltrami operator assumes the form of a $n \times n$ matrix $\Delta = \mathbf{A}^{-1}\mathbf{W}$, where \mathbf{A} is a diagonal matrix of local area elements $a_i = \frac{1}{3} \sum_{j,k:i,j,k \in F} A_{ijk}$, and \mathbf{W} is a symmetric matrix of edge-wise weights, defined in terms of the discrete metric as¹:

$$w_{ij} = \begin{cases} \frac{-\ell_{ij}^2 + \ell_{jk}^2 + \ell_{ki}^2}{8A_{ijk}} + \frac{-\ell_{ij}^2 + \ell_{jh}^2 + \ell_{hi}^2}{8A_{ijh}} & \text{if } e_{ij} \in E_i \\ \frac{-\ell_{ij}^2 + \ell_{jh}^2 + \ell_{hi}^2}{8A_{ijh}} & \text{if } e_{ij} \in E_b \\ -\sum_{k \neq i} w_{ik} & \text{if } i = j \end{cases} \quad (6)$$

This discretization clearly depends on the mesh connectivity (encoded by edges E and triangles F) and on the vertex coordinates \mathbf{V} (via the lengths ℓ_{ij}); since both play important roles in our reconstruction problem, we make this dependency explicit by writing $\Delta_X(\mathbf{V})$.

¹It can be easily shown that this discretization is equivalent to the classical cotangent formulas [22], see e.g. [17].

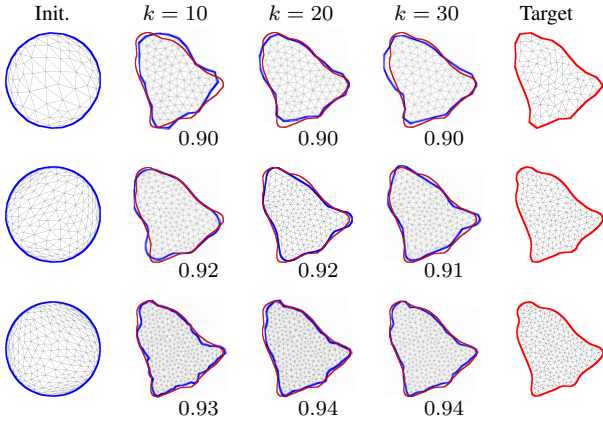


Figure 3. Shape recovery at increasing mesh resolution ($n = 100, 200,$ and 300 vertices increasing top to bottom) and bandwidth ($k = 10, 20,$ and 30 eigenvalues increasing left to right). In each test, the mesh graph *connectivity* of the target is known and input to the optimization process. We report the IOU score below each reconstruction. A finer sampling significantly improves the performance of the algorithm, whereas extending the bandwidth above $k = 30$ does not seem to improve quality any further.

4. Isospectralization

Our approach builds upon the assumption that knowledge of a limited portion of the spectrum is enough to fix the shape of the domain, given some minimal amount of additional information which we phrase as simple regularizers. We consider inverse problems of this form:

$$\min_{\mathbf{V} \in \mathbb{R}^{n \times d}} \|\boldsymbol{\lambda}(\boldsymbol{\Delta}_X(\mathbf{V})) - \boldsymbol{\mu}\|_{\omega} + \rho_X(\mathbf{V}), \quad (7)$$

where \mathbf{V} is the (unknown) embedding of the mesh vertices in \mathbb{R}^d , $\boldsymbol{\Delta}_X(\mathbf{V})$ is the associated discrete Laplace-Beltrami operator, $\|\cdot\|_{\omega}$ is a weighted norm defined below, and $\boldsymbol{\mu}, \boldsymbol{\lambda} \in \mathbb{R}_+^k$ respectively denote the input sequence and the first k eigenvalues of $\boldsymbol{\Delta}_X(\mathbf{V})$. Function ρ_X is a regularizer for the embedding, implementing the natural expectation that the sought solution should satisfy certain desirable properties.

Note that using a standard ℓ_2 norm in the definition of the energy (7) would not lead to accurate shape recovery. This is due to the fact that, since the high end of the spectrum accounts for small geometric variations of the embedding, a local optimum can be reached by perfectly aligning the high frequencies and concentrating most of the alignment error on the lower end (which accounts for the more global shape appearance). To make error diffusion more balanced, we thus adopt the weighted norm

$$\|\boldsymbol{\lambda} - \boldsymbol{\mu}\|_{\omega} = \sum_{i=1}^k \frac{1}{i} (\lambda_i - \mu_i)^2. \quad (8)$$

Problem (7) seeks a Euclidean embedding whose Laplacian eigenvalues align to the ones given as input. From an

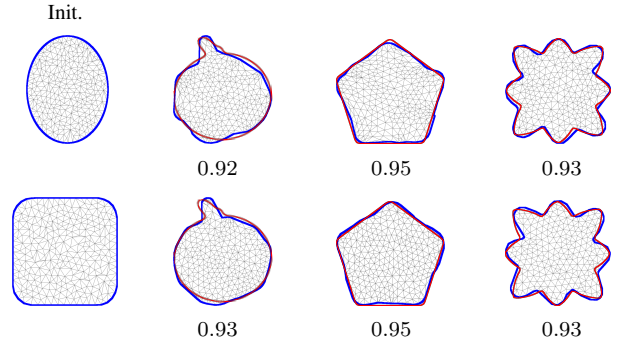


Figure 4. Shape recovery with unknown mesh connectivity, under two different initializations. We report the IOU score below each recovered embedding. In these tests, the mesh tessellation used in the optimization was chosen arbitrarily and is in no way related to the input sequence of eigenvalues.

optimization perspective, this problem is particularly difficult since 1) the optimization variables are nested, and 2) the problem is highly non-linear and thus susceptible to local minima. As we show in the sequel, however, in all our tests we observed almost perfect alignment of the spectra; we refer to the implementation Section 4.3 for further details.

4.1. Flat shapes

When the embedding space is \mathbb{R}^2 , a shape \mathcal{X} is entirely determined by its boundary $\partial\mathcal{X}$. For this reason, we consider a variant of Problem (7) where we optimize only for the boundary vertices.

Regularizers. We adopt the composite penalty

$$\rho_X(\mathbf{V}) = \rho_{X,1}(\mathbf{V}) + \rho_{X,2}(\mathbf{V}), \quad (9)$$

where $\rho_{X,1}(\mathbf{V})$ is a smoothness-promoting term

$$\rho_{X,1}(\mathbf{V}) = \sum_{e_{ij} \in E_b} \ell_{ij}^2(\mathbf{V}). \quad (10)$$

and $\rho_{X,2}(\mathbf{V})$ is defined as:

$$\rho_{X,2}(\mathbf{V}) = \left(\sum_{ijk \in F} (\mathbf{R}_{\frac{\pi}{2}}(\mathbf{v}^j - \mathbf{v}^i))^{\top} (\mathbf{v}^k - \mathbf{v}^i) \right)_-, \quad (11)$$

where $\mathbf{R}_{\frac{\pi}{2}} = \begin{pmatrix} 0 & -1 \\ 1 & 0 \end{pmatrix}$ rotates 2D vectors by $\frac{\pi}{2}$ and $(x)_- = (\min\{0, x\})^2$. This term penalizes triangle flips that may occur throughout the optimization, and works under the assumption of clockwise oriented triangles.

Error measure. We quantify the reconstruction quality as the area ratio of the intersection of the recovered and target embeddings over their union (IOU, the higher the better) after an optimal alignment has been carried out. In our plots, we visualize the recovered embedding with a blue outline, and the ground-truth (unknown) target with a red outline.

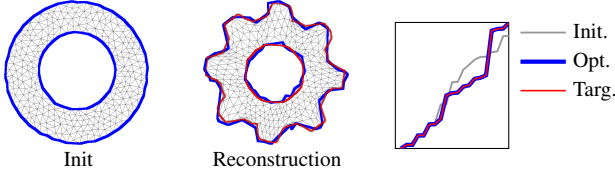


Figure 5. Reconstruction of a non-simply connected shape. On the right we also show the initial, target, and optimized spectra.

Mesh resolution and bandwidth. By operating with a discrete Laplace operator, our optimization problem is directly affected by the quality of the discretization. We investigate this dependency by running an evaluation at varying mesh resolution (in terms of number of vertices) and spectral bandwidth (number k of input eigenvalues). The results are reported in Figure 3.

Examples. In Figure 4 we show additional reconstruction results for different shapes. We remark that, differently from the previous tests, in these experiments we do *not* assume the mesh connectivity to be known. This way we put ourselves in the most general setting where the only input information is represented by the eigenvalues, thus factoring out any geometric aid that might be implicitly encoded in the connectivity graph.

Topology. At no point in our pipeline we assume the manifolds to be simply-connected. An example of recovery of a shape with a hole is given in Figure 5. We do assume, however, to know the topological class (*e.g.*, annulus-like rather than disc-like) of the target.

4.2. Surfaces

In the more general case of embeddings in \mathbb{R}^3 we once again adopt a composite penalty $\rho_X(\mathbf{V}) = \rho_{X,1}(\mathbf{V}) + \rho_{X,2}(\mathbf{V})$ with two different regularizers.

The first regularizer promotes vertices to lie on the barycenter of their one-ring neighbors. It is defined as:

$$\rho_{X,1}(\mathbf{V}) = \|\mathbf{L}\mathbf{V}\|_F^2, \quad (12)$$

where \mathbf{L} is the graph Laplacian of the initial embedding. This term has the effect of promoting both a smooth surface and a more uniformly sampled embedding.

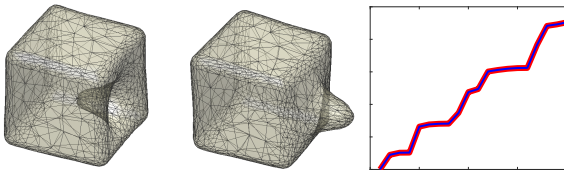


Figure 6. Two isometric shapes with different volume; their (identical) spectra are shown on the right. Our volume regularizer allows to disambiguate the two solutions.

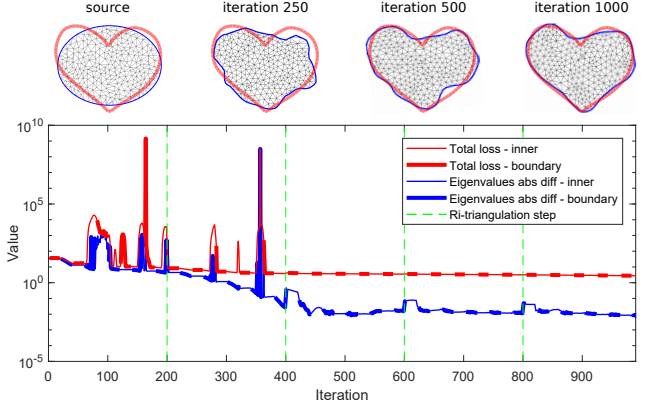


Figure 7. Energy plot during our alternating optimization process for flat shapes. Spikes in the energy are due to the triangle flip penalty. Note how the optimization is able to recover from ugly triangulated embeddings (*i.e.*, flipped triangles) and reach a stable minimum very close to a global optimum.

The second regularizer is a volume expansion term where the shape volume is estimated via the (discrete) divergence theorem as:

$$\rho_{X,2}(\mathbf{V}) = \left(\frac{1}{1}\right)^\top \sum_{ijk \in F} ((\mathbf{v}^j - \mathbf{v}^i) \times (\mathbf{v}^k - \mathbf{v}^j)) (\mathbf{v}^i + \mathbf{v}^j + \mathbf{v}^k). \quad (13)$$

This term is useful in disambiguating isometries which differ by a change in volume (see Figure 6).

4.3. Implementation details

In implementing the described optimization there are some technicalities that need to be taken into account, mostly due to ugly triangulations of the embedding that could occur during the minimization.

In the flat shape scenario, even if we optimize (7) only over boundary edges, the interior vertices need to be repositioned so as to preserve a regular sampling of the shape. We do so by means of an alternating optimization: First, the contour points are optimized; this is followed by a relocation of the interior points according to a squared edge length minimization strategy. In order to avoid the creation of degenerate triangles, we also perform a resampling step in which a new triangulation is recomputed while preserving boundary edges. Even if there are no guarantees for the alternating optimization to converge, we always observed convergence in all our experiments. An example of the behavior of the energy during minimization is shown in Figures 7 and 8.

For the numerical optimization we leverage auto-differentiation and optimization tools from the field of deep learning. We used the Adam [21] optimizer implementation of Tensorflow adopting a cosine decay strategy of the regularizer weights. For flat shapes, we alternate optimization of boundary and interior points every 10 iterations, while

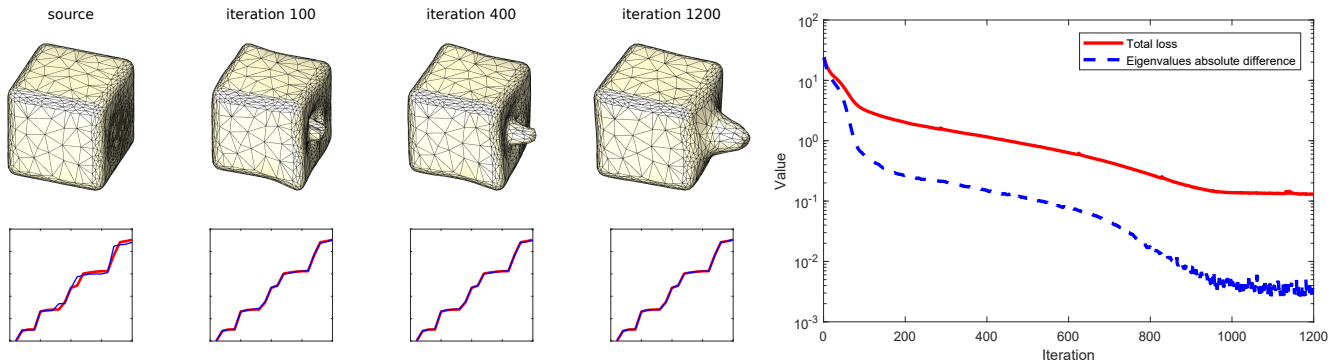


Figure 8. An example of the reconstruction process; the target is a cube with a bump similar to the solution at iteration 1200. The plots under each shape show the current eigenvalues alignment (the target is the blue curve). Observe the staircase-like pattern due to the symmetry of the cube.

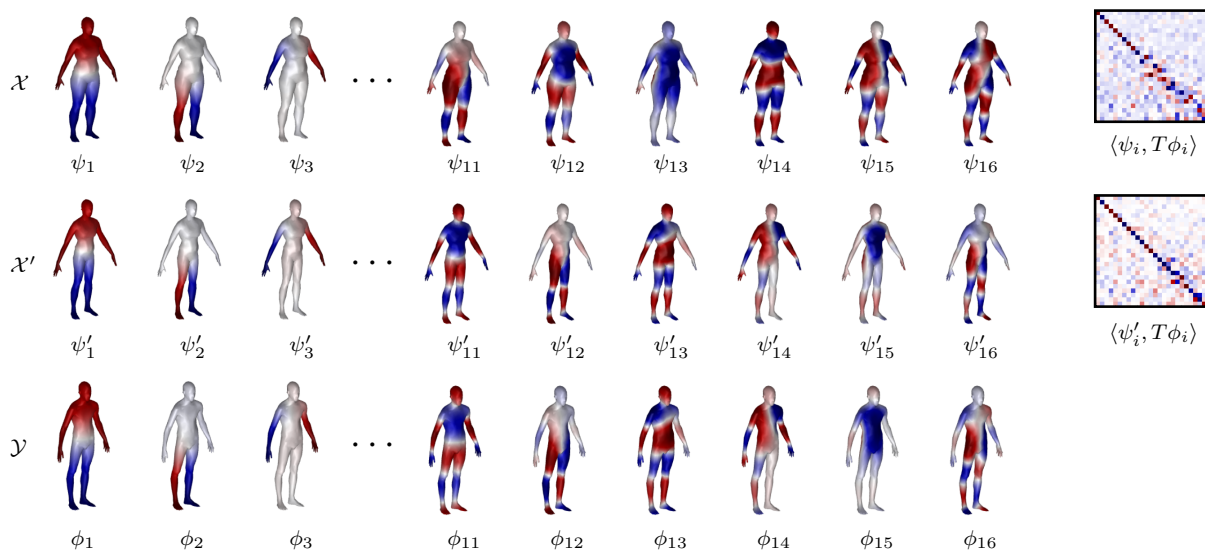


Figure 9. Eigenfunctions alignment and shape deformation as a result of isospectralization for non-isometric shape matching. Starting from a source shape \mathcal{X} (first row), our algorithm solves for an embedding \mathcal{X}' (middle row) having the same Laplacian eigenvalues as those of the target \mathcal{Y} . Note how the eigenvalue alignment induces an alignment of the corresponding eigenfunctions, making the pairs (ψ'_i, ϕ_i) more similar than the initial pairs (ψ_i, ϕ_i) . This is reflected in more diagonal functional map matrices (rightmost column), which in turn leads to a better conditioning for shape matching algorithms.

a resampling step is performed once every 2000 iterations. Where not differently specified, we optimize for the first 30 eigenvalues in both flat shapes and surfaces, resampled respectively to 400 and 1000 points.

5. Applications in shape analysis

5.1. Non-isometric shape matching

We have applied our shape optimization approach to the problem of finding correspondences between non-rigid shapes. In this setting, we are given a pair of 3D shapes \mathcal{X}, \mathcal{Y} , both represented as triangle meshes, and our goal is to find a dense map $T : \mathcal{X} \rightarrow \mathcal{Y}$ between them. This is a very well-studied problem in computer vision and computer graphics, with a wide range of techniques proposed over the

years (see [33, 32, 5] for several surveys).

Non-rigid shape matching is particularly difficult, as it would require designing a universal correspondence algorithm, capable of handling arbitrary deformations in a fully automatic way. A very successful sub-class of non-rigid shape deformations is *intrinsic isometries*, in which the underlying map T is assumed to approximately preserve *geodesic distances* between pairs of points on the shapes. A large number of efficient methods has been proposed to solve the shape matching problem under this assumption [5]. At the same time, most of these techniques result in very poor correspondences whenever the assumption of intrinsic isometry is not satisfied.

Approach. Our main insight is that the alignment of the

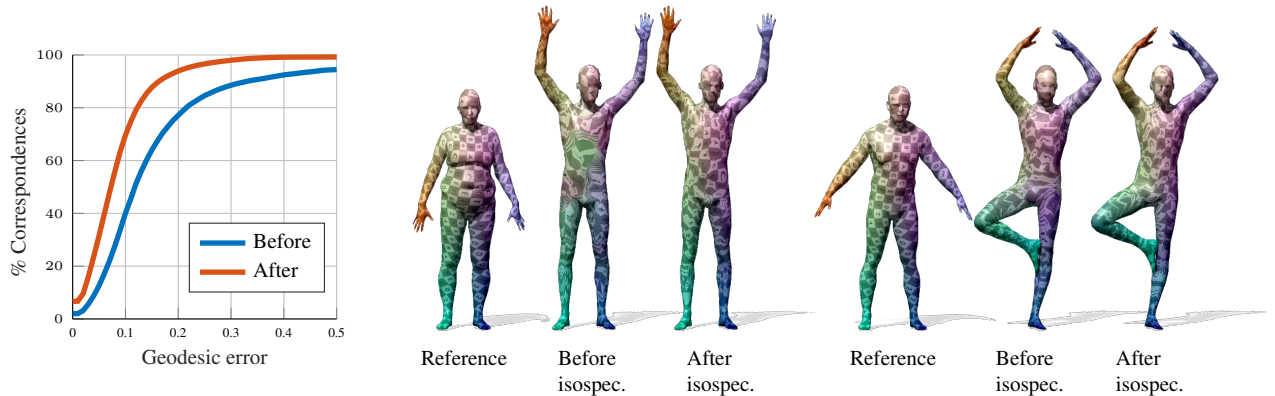


Figure 10. Results on the non-isometric shape matching application. The plots shown on the left are averaged over a set of 60 non-isometric shape pairs from the FAUST inter-subject dataset [6]. In order to visualize correspondence, we use it to transfer a texture from source to target.

spectra of the two shapes can help them make more intrinsically isometric, and thus can facilitate finding accurate correspondences using existing techniques. Namely, given shapes \mathcal{X}, \mathcal{Y} , with Laplacian spectra $\lambda_{\mathcal{X}}, \lambda_{\mathcal{Y}}$ we propose to find correspondences between them using the following three-step approach:

1. Deform \mathcal{X} to obtain \mathcal{X}' whose spectrum $\lambda_{\mathcal{X}'}$ is better aligned with $\lambda_{\mathcal{Y}}$.
2. Compute the correspondence $T' : \mathcal{X}' \rightarrow \mathcal{Y}$ using an existing isometric shape matching algorithm.
3. Convert T' to $T : \mathcal{X} \rightarrow \mathcal{Y}$ using the identity map between \mathcal{X} and \mathcal{X}' .

Our main intuition is that as mentioned above, despite the existence of exceptional counter-examples, in most practical cases this procedure is very likely to make shapes \mathcal{X}' and \mathcal{Y} close to being isometric. Therefore, we would expect an isometric shape matching algorithm to match \mathcal{Y} to \mathcal{X}' better than to the original shape \mathcal{X} . Finally, after computing a map $T : \mathcal{X}' \rightarrow \mathcal{Y}$, we can trivially convert it to a map, since $\mathcal{X}, \mathcal{X}'$ are in 1-1 correspondence.

The approach described above builds upon the remarkable observation that aligning the Laplacian eigenvalues also induces an alignment of the *eigenspaces* of the two shapes. This is illustrated on a real example in Figure 9, where we show a subset of eigenfunctions for two non-isometric surfaces (a man and a woman) before and after isospectralization. In a sense, isospectralization implements a notion of *correspondence-free* alignment of the functional spaces spanned by the set of the first k Laplacian eigenfunctions.

Implementation. For these tests, we replaced the optimization variables by optimizing over a *displacement field* rather than the absolute vertex positions in Problem (7). This allows us to better preserve the geometric details of the initial

shape and thus yield a better transfer of the overall style as encoded in the lower frequencies.

We have implemented the approach described above by using an existing shape correspondence algorithm [24] based on the functional maps framework [25, 26]. One of the advantages of this approach is that it is *purely intrinsic* and only depends on the quantities derived from the Laplace-Beltrami operators of the two shapes. Note that the exact embedding of the optimized shape \mathcal{X}' does not play a role, and can be different from that of \mathcal{Y} . In other words, we do not aim to reproduce the shape \mathcal{Y} , but rather only use our shape optimization strategy as an auxiliary step to facilitate shape correspondence.

Specifically, we use the functional maps-based algorithm of [24] with the open source implementation provided by the authors. This algorithm is based on first solving for a functional map between a pair of shapes, using several descriptor-preservation and regularization constraints, and then converting the functional map to a pointwise one. As done in the implementation of [24], we used the wave kernel signature [2] as descriptors and commutativity with the Laplace-Beltrami operators for map regularization. This leads to a convex optimization problem for functional map inference, which can be efficiently solved with an iterative quasi-Newton method. Finally, we convert a functional map to a pointwise one using a simple nearest neighbor search in the spectral domain, as proposed in [25]. In all cases, we evaluate the quality of the final correspondence by measuring the average geodesic error with respect to some externally-provided ground truth map [20]. We refer to Figures 1 (bottom row), 10, 11, and 12 for quantitative and qualitative results.

5.2. Style transfer

As a second possible application we explore the task of style transfer between deformable shapes. Given a pair of

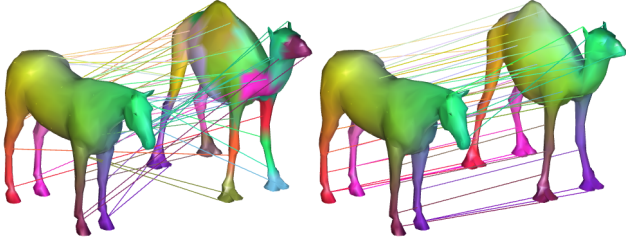


Figure 11. Non-isometric shape matching before (left) and after (right) isospectralization. The correspondence is computed according to the algorithm of Section 5.1.

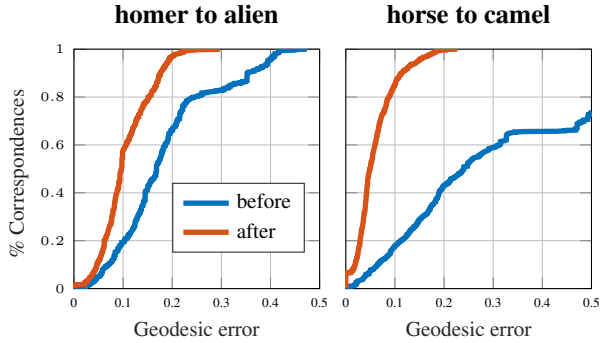


Figure 12. Quantitative evaluation of non-isometric shape matching for the homer/alien pair of Figure 1 and the horse/camel pair of Figure 11. Isospectralization leads to a dramatic improvement in correspondence accuracy.

surfaces \mathcal{X} (the source) and \mathcal{Y} (the target), the idea is to modify the medium-to-high frequency details of \mathcal{X} to match those of shape \mathcal{Y} , while maintaining its overall pose in space as encoded in the lower-end portion of $\lambda_{\mathcal{X}}$. We do so simply by recovering an embedding in \mathbb{R}^3 from the eigenvalues $\lambda_{\mathcal{Y}}$, where we initialize the optimization with the source shape \mathcal{X} . Qualitative examples of this procedure are shown in Figure 13.

We emphasize that this way of transferring geometric details among two given surfaces is completely correspondence-free, as it does *not* require the notion of a map between the input shapes. This is different from existing approaches like [8], which in addition to requiring the entire Laplacian matrix, also require a precise map between \mathcal{X} and \mathcal{Y} to be given as input.

6. Discussion and conclusions

“Vibrations are everywhere, and so too are the eigenvalues associated with them.” (Parlett, 1998)

In this paper, we addressed the decades-old problem of recovering a metric embedding from a (partial) measurement of its Laplacian eigenvalues by introducing a numerical procedure called isospectralization, trying to deform the shape embedding to align its Laplacian eigenvalues with

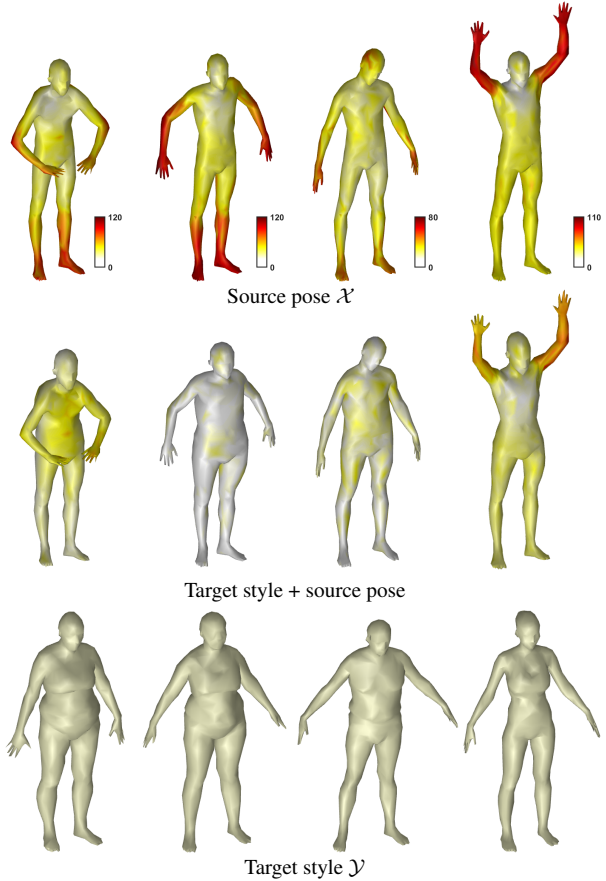


Figure 13. Spectra alignment can be used to implement a notion of style transfer between shapes. In these four examples (one per column), we transfer the style of the target shape (third row) to the source shape (first row), obtaining the embeddings shown in the middle. The colored heatmap encodes distortion of the geodesic distances, growing from white to dark red.

a given spectrum. We find it remarkable that the use of isospectralization simplifies the problem of finding intrinsic correspondences between shapes, allowing to significantly improve standard pipelines for shape matching almost for free. Interestingly, there is no *a priori* guarantee that the isospectralization process deforms the shapes in a sensible way (for instance, it is conceivable that isospectralizing a horse into a camel would result in the horse’s legs collapsing while a new set grows out of its back, which would spoil the construction of the correspondence). Our results suggest that such situations do not arise in practice when using a gradient descent-like algorithm that deforms the shape progressively. In other words, our approach to isospectralization deforms the shape in a meaningful way. It would be of interest to obtain a mathematically precise statement of this meaningfulness. This would be of both practical importance in shape matching and, potentially, mathematical interest in the field of spectral geometry.

References

- [1] D. Aasen, T. Bhamre, and A. Kempf. Shape from sound: toward new tools for quantum gravity. *Physical Review Letters*, 110(12):121301, 2013. 3
- [2] M. Aubry, U. Schlickewei, and D. Cremers. The Wave Kernel Signature: A Quantum Mechanical Approach to Shape Analysis. In *Proc. ICCV Workshops*, 2011. 7
- [3] M. Berger. *A panoramic view of Riemannian geometry*. Springer Science & Business Media, 2012. 2
- [4] G. Bharaj, D. I. Levin, J. Tompkin, Y. Fei, H. Pfister, W. Matusik, and C. Zheng. Computational design of metallophone contact sounds. *TOG*, 34(6), 2015. 3
- [5] S. Biasotti, A. Cerri, A. Bronstein, and M. Bronstein. Recent trends, applications, and perspectives in 3d shape similarity assessment. *Computer Graphics Forum*, 35(6):87–119, 2016. 6
- [6] F. Bogo, J. Romero, M. Loper, and M. J. Black. FAUST: Dataset and Evaluation for 3d Mesh Registration. In *Proc. CVPR*, 2014. 7
- [7] V. Borrelli, S. Jabrane, F. Lazarus, and B. Thibert. Flat tori in three-dimensional space and convex integration. *PNAS*, 2012. 2
- [8] D. Boscaini, D. Eynard, D. Kourounis, and M. M. Bronstein. Shape-from-operator: Recovering shapes from intrinsic operators. *Computer Graphics Forum*, 34(2):265–274, 2015. 2, 8
- [9] A. Chern, F. Knöppel, U. Pinkall, and P. Schröder. Shape from metric. *TOG*, 37(4):63:1–63:17, 2018. 2
- [10] M. Chu and G. Golub. *Inverse eigenvalue problems: theory, algorithms, and applications*. Oxford University Press, 2005. 2, 3
- [11] E. Corman, J. Solomon, M. Ben-Chen, L. Guibas, and M. Ovsjanikov. Functional characterization of intrinsic and extrinsic geometry. *TOG*, 36(2):14, 2017. 2
- [12] C. Gordon, D. Webb, and S. Wolpert. Isospectral plane domains and surfaces via Riemannian orbifolds. *Inventiones Mathematicae*, 110(1):1–22, 1992. 1
- [13] C. Gordon, D. L. Webb, and S. Wolpert. One cannot hear the shape of a drum. *Bulletin of the American Mathematical Society*, 27:134–138, 1992. 1, 2
- [14] H. Hamidian, J. Hu, Z. Zhong, and J. Hua. Quantifying shape deformations by variation of geometric spectrum. In *Proc. MICCAI*, 2016. 2
- [15] H. Hezari and S. Zelditch. Inverse Spectral Problem for Analytic $(\mathbb{Z}/2\mathbb{Z})$ -Symmetric Domains in \mathbb{R}^N . *Geometric and Functional Analysis*, 20(1):160–191, 2010. 1
- [16] J. Hu, H. Hamidian, Z. Zhong, and J. Hua. Visualizing shape deformations with variation of geometric spectrum. *IEEE TVCG*, 23(1):721–730, 2017. 2
- [17] A. Jacobson and O. Sorkine-Hornung. A cotangent laplacian for images as surfaces. *Technical report/Department of Computer Science, ETH, Zurich*, 757, 2012. 3
- [18] M. Kac. Can one hear the shape of a drum? *The American Mathematical Monthly*, 73(4):1–23, 1966. 1, 2
- [19] A. Kempf. Spacetime could be simultaneously continuous and discrete, in the same way that information can be. *New Journal of Physics*, 12(11):115001, 2010. 2
- [20] V. G. Kim, Y. Lipman, and T. Funkhouser. Blended Intrinsic Maps. *TOG*, 30(4):79, 2011. 7
- [21] D. P. Kingma and J. Ba. Adam: A method for stochastic optimization. *CoRR*, abs/1412.6980, 2014. 5
- [22] M. Meyer, M. Desbrun, P. Schröder, and A. H. Barr. Discrete differential-geometry operators for triangulated 2-manifolds. In *Visualization and Mathematics III*, pages 35–57. Springer, 2003. 3
- [23] J. Milnor. Eigenvalues of the Laplace operator on certain manifolds. *PNAS*, 51(4):542, 1964. 1, 2
- [24] D. Nogneng and M. Ovsjanikov. Informative descriptor preservation via commutativity for shape matching. *Computer Graphics Forum*, 36(2):259–267, 2017. 7
- [25] M. Ovsjanikov, M. Ben-Chen, J. Solomon, A. Butscher, and L. Guibas. Functional Maps: A Flexible Representation of Maps Between Shapes. *TOG*, 31(4):30, 2012. 7
- [26] M. Ovsjanikov, E. Corman, M. Bronstein, E. Rodolà, M. Ben-Chen, L. Guibas, F. Chazal, and A. Bronstein. Computing and processing correspondences with functional maps. In *SIGGRAPH Courses*, pages 5:1–5:62, 2017. 7
- [27] M. Panine and A. Kempf. Towards spectral geometric methods for euclidean quantum gravity. *Physical Review D*, 93(8):084033, 2016. 3
- [28] M. Reuter, F.-E. Wolter, and N. Peinecke. Laplace-spectra as fingerprints for shape matching. In *Proc. SPM*, SPM '05, pages 101–106, New York, NY, USA, 2005. ACM. 2
- [29] M. Reuter, F.-E. Wolter, and N. Peinecke. Laplace-beltrami spectra as 'shape-dna' of surfaces and solids. *Computer Aided Design*. 38(4):342–366, Apr. 2006. 2
- [30] S. C. Schonsheck, M. M. Bronstein, and R. Lai. Nonisometric surface registration via conformal laplace-beltrami basis pursuit. *arXiv:1809.07399*, 2018. 2
- [31] O. Sorkine and D. Cohen-Or. Least-squares meshes. In *Proc. Shape Modeling Applications, 2004. Proceedings*, pages 191–199, 2004. 2
- [32] G. K. Tam, Z.-Q. Cheng, Y.-K. Lai, F. C. Langbein, Y. Liu, D. Marshall, R. R. Martin, X.-F. Sun, and P. L. Rosin. Registration of 3d point clouds and meshes: a survey from rigid to nonrigid. *IEEE Trans. Visualization and Computer Graphics*, 19(7):1199–1217, 2013. 6
- [33] O. Van Kaick, H. Zhang, G. Hamarneh, and D. Cohen-Or. A survey on shape correspondence. In *Computer Graphics Forum*, volume 30, pages 1681–1707, 2011. 6
- [34] H. Weyl. Über die asymptotische Verteilung der Eigenwerte. *Nachrichten von der Gesellschaft der Wissenschaften zu Göttingen, Mathematisch-Physikalische Klasse*, pages 110–117, 1911. 3
- [35] S. Zelditch. The inverse spectral problem for surfaces of revolution. *J. Diff. Geom.*, 49(2):207–264, 1998. 1
- [36] S. Zelditch. Spectral determination of analytic bi-axisymmetric plane domains. *Geometric & Functional Analysis GAFA*, 10(3):628–677, 2000. 1
- [37] S. Zelditch. Inverse Spectral Problem for Analytic Domains, II: \mathbb{Z}_2 -symmetric domains. *Annals of Mathematics*, 170(1):205–269, 2009. 1